



Simultaneous evaluation of perfusion and morphology using GRASP MRI in hepatic fibrosis

Jeong Hee Yoon^{1,2} · Jeong Min Lee^{1,2,3} · Mi Hye Yu⁴ · Bo Yun Hur⁵ · Robert Grimm⁶ · Steven Sourbron⁷ · Hersh Chandarana^{8,9} · Yohan Son¹⁰ · Susmita Basak¹¹ · Kyoung-Bun Lee¹² · Nam-Joon Yi¹³ · Kwang-Woong Lee¹³ · Kyung-Suk Suh¹³

Received: 28 January 2021 / Revised: 11 May 2021 / Accepted: 20 May 2021 / Published online: 12 June 2021

© European Society of Radiology 2021

Abstract

Objectives To determine if golden-angle radial sparse parallel (GRASP) dynamic contrast-enhanced (DCE)-MRI allows simultaneous evaluation of perfusion and morphology in liver fibrosis.

Methods Participants who were scheduled for liver biopsy or resection were enrolled (NCT02480972). Images were reconstructed at 12-s temporal resolution for morphologic assessment and at 3.3-s temporal resolution for quantitative evaluation. The image quality of the morphologic images was assessed on a four-point scale, and the Liver Imaging Reporting and Data System score was recorded for hepatic observations. Comparisons were made between quantitative parameters of DCE-MRI for the different fibrosis stages, and for hepatocellular carcinoma (HCCs) with different LR features.

Results DCE-MRI of 64 participants (male = 48) were analyzed. The overall image quality consistently stood at 3.5 ± 0.4 to 3.7 ± 0.4 throughout the exam. Portal blood flow significantly decreased in participants with F2–F3 ($n = 18$, 175 ± 110 mL/100 mL/min) and F4 ($n = 12$, 98 ± 47 mL/100 mL/min) compared with those in participants with F0–F1 ($n = 34$, 283 ± 178 mL/100 mL/min, $p < 0.05$ for all). In participants with F4, the arterial fraction and extracellular volume were significantly higher than those in participants with F0–F1 and F2–F3 ($p < 0.05$). Compared with HCCs showing non-LR-M features ($n = 16$), HCCs with LR-M ($n = 5$) had a significantly prolonged mean transit time and lower arterial blood flow ($p < 0.05$).

Conclusions Liver MRI using GRASP obtains both sufficient spatial resolution for confident diagnosis and high temporal resolution for pharmacokinetic modeling. Significant differences were found between the MRI-derived portal blood flow at different hepatic fibrosis stages.

Key Points

- A single MRI examination is able to provide both images with sufficient spatial resolution for anatomic evaluation and those with high temporal resolution for pharmacokinetic modeling.
- Portal blood flow was significantly lower in clinically significant hepatic fibrosis and mean transit time and extracellular volume increased in cirrhosis, compared with those in no or mild hepatic fibrosis.
- HCCs with different LR features showed different quantitative parameters of DCE-MRI: longer mean transit time and lower arterial flow were observed in HCCs with LR-M features.

Keywords Liver · Magnetic resonance imaging · Liver cirrhosis · Carcinoma · hepatocellular

Abbreviations

AF Arterial fraction
AIF Arterial input function

AUC Area under the curve
DCE Dynamic contrast-enhanced
ECV Extracellular volume
GRASP Golden-angle radial sparse parallel
HCC Hepatocellular carcinoma
ICC Intraclass correlation coefficient
LI-RADS Liver Imaging Reporting and Data System
LOA Limit of agreement
MRI Magnetic resonance imaging

✉ Jeong Min Lee
jmsh@snu.ac.kr

Extended author information available on the last page of the article

MTT	Mean transit time
T1WI	T1-weighted image
VIF	Venous input function

Introduction

To measure tissue perfusion non-invasively, various perfusion imaging techniques are used including dynamic contrast-enhanced magnetic resonance imaging (DCE-MRI) [1–3]. However, DCE-MRI has been limitedly utilized in the evaluation of liver parenchyma and liver tumors [4–6]. It is because that DCE-MRI requires high temporal resolution to trace dynamic changes in tissue signal intensity and vascular enhancement peak [7, 8]. To achieve high temporal resolution, spatial resolution and image quality are often compromised. Moreover, data are often contaminated by motion artifact in liver imaging. Thus, DCE-MRI is often unable to provide the requisite diagnostic image quality for clinical purpose. As a result, patients need to undergo contrast-enhanced MRI twice to obtain functional information additionally, which is cumbersome for the patients and the workflow in the hospital. If we are able to obtain morphologic imaging and measure liver perfusion simultaneously, it would be helpful implementing DCE-MRI in clinical practice.

Golden-angle radial sparse parallel (GRASP) MRI is a technique which combines parallel imaging, radial acquisition, and compressed sensing [9]. It speeds up the scan time by using compressed sensing and parallel imaging concurrently, and it is less sensitive to motion owing to its radial acquisition scheme [10]. Furthermore, its golden-angle sampling schemes afford flexibility in the temporal resolution which in turn permits retrospective reconstruction of image series at different temporal resolutions from a single acquisition dataset [11]. Therefore, the purpose of our study is to evaluate liver perfusion and morphology simultaneously at GRASP DCE-MRI in patients with hepatic fibrosis.

Materials and methods

This prospective study was performed after approval by our Institutional Review Board, and written informed consent was obtained from all participants (NCT02480972).

From June 2015 to September 2016, participants who met the following eligibility criteria were enrolled: they (a) had liver cirrhosis or chronic viral hepatitis or (b) were living liver donor candidates, and (c) were scheduled for liver biopsy, resection, or transplantation, and (d) had signed informed consent. The exclusion criteria were as follows: (a) being younger than 18 years and (b) having absolute/relative contraindications to DCE-MRI such as having cardiac implantable

electronic devices, cochlear implants, metallic fragments or prosthesis, moderate to severe degree of adverse reaction to gadolinium, acute or chronic renal failure (eGFR < 30 mL/min/1.73 m²), nursing, or pregnancy. Sex, age, underlying disease, pathology results, and laboratory findings including albumin, total bilirubin, prothrombin time, and hematocrit level were recorded. The presence or absence of esophageal varix was recorded from endoscopy within 3 months of enrollment.

MRI acquisition

All examinations were performed with a 3-T scanner (MAGNETOM Skyra, Siemens Healthineers) using a standard 48-channel phased array body coil. DCE-MRI was obtained in axial plane using GRASP as described below. Details of liver MRI are described in Supplementary information.

Participants were asked to relax and breathe regularly. A T1-weighted image (T1WI) was obtained using a prototype 3D gradient-echo GRASP MRI pulse sequence in a free-breathing manner for 60 s (406 radial spokes) and 4 min (1852 radial spokes) before and after administration of contrast media (0.1 mmol/kg, Gadovist, Bayer) at a rate of 1.5 mL/s followed by a 20-mL saline chaser. The number of slices ranged from 64 to 72, covering the whole liver. The field of view was 450 × 450 mm, with a matrix of 256 × 256, and the voxel size was 1.75 × 1.75 × 3 mm³ (Table E1).

Prototype software was used to retrospectively reconstruct the acquired GRASP k-space data at different temporal resolutions. For morphologic evaluation, images were reconstructed using 84 spokes and respiratory gating (acceptance window 0.5), corresponding to a temporal resolution of 12 s [11]. For DCE-MRI, GRASP data were reconstructed using 21 spokes which resulted in 3.3 s of temporal resolution.

Qualitative image analysis

One board-certified radiologist who did not attend the qualitative review session chose one precontrast, one arterial, one portal-venous, and one delayed phase reconstruction from the reconstructed series with a 12-s temporal resolution, considering the timing and degrees of artifacts. In addition, this radiologist evaluated the presence or absence of varices at MRI.

Three fellowship-trained abdominal radiologists (J.H.Y., M.H.Y., B.Y.H.) independently reviewed the chosen images. Motion artifacts, streak artifacts, liver edge sharpness, and overall image quality were assessed on a four-point scale with a higher score indicating better image quality. Motion and streak artifacts were assessed as follows: 1 = severe artifacts hindering the diagnostic capability, 2 = moderate artifacts with decreased image quality without diagnostic performance

impairment, 3 = mild artifacts without significant image quality disturbance, and 4 = no perceivable artifacts. Liver edge sharpness was scored as follows: 1 = extreme blur, 2 = a partially indistinctive liver margin with moderate blur, 3 = slightly soft liver margin with mild blur, and 4 = clear liver margin and minimal blur. The overall image quality was assessed as follows: 1 = non-diagnostic; 2 = unsatisfactory image quality, but re-examination not required; 3 = acceptable image quality; and 4 = comparable with average breath-hold image quality. Lastly, reviewers evaluated non-cystic hepatic observations (≥ 10 mm) according to the Liver Imaging Reporting and Data System (LI-RADS) version 2018 [12]. The final LR-score was determined as the score at least two reviewers reported.

DCE-MRI analysis

DCE-MRI data of 3.3-s temporal resolution were analyzed with freely available software (PMI 04, Platform for Research in Medical Imaging) written in IDL 6.0 (ITT, Boulder) [13]. Modeling and analysis followed similar principles as previous studies [13, 14].

Arterial and portal-venous regions of interest (ROIs) were defined semi-automatically over two to four slices by thresholding a map of maximum signal enhancement followed by manual identification of the aorta and portal vein, respectively. In order to reduce the inflow effect in the arterial input function (AIF), a map of maximum signal change over time was created and an aorta ROI was selected in a slice where this was minimal. Liver ROIs were drawn manually in the periphery of the liver parenchyma, avoiding large vessels and hepatic observations over four slices by one fellowship-trained radiologist (J.H.Y.). AIF, venous input function (VIF), and tissue curves were extracted by averaging the signal values in the

respective ROIs for each time point. In order to assess inter-observer agreement, another fellowship-trained radiologist (J.M.L.) performed DCE-MRI analysis in the same manner. Volumetric segmentation was also performed for treatment-naïve non-cystic observations (≥ 10 mm).

Contrast agent concentration $C(t)$ was derived from the signal-time curves $S(t)$, assuming a linear relation between signal and concentration:

$$C(t) = \frac{1}{r_1 T_{10}} \frac{S(t) - S_0}{S_0}$$

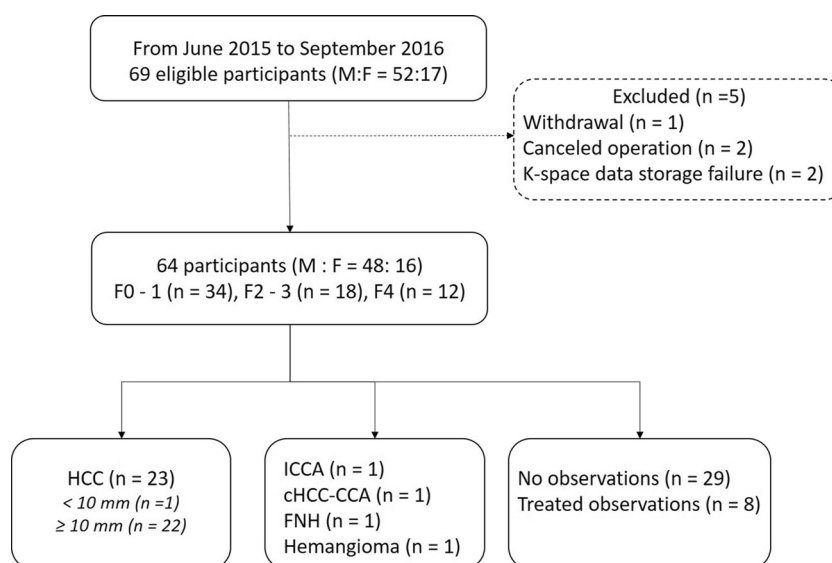
where S_0 is the signal intensity in the precontrast phase, r_1 is the relaxivity of the contrast agent (3.6/s/mmol), and T_{10} is the precontrast T1 [15]. For the liver, T1 was fixed to the literature value of 809 ms [16]. For arterial and venous blood, T1 values (s) were chosen as $1.0 / (0.52 \text{ Hct} + 0.38)$ and $1.0 / (0.83 \text{ Hct} + 0.28)$, respectively [17], where Hct is the subject-specific hematocrit. Plasma concentration for AIF and VIF was derived by dividing the blood concentrations by (1-Hct).

A delayed, dual-inlet one-compartment model was fitted to the concentrations.

$$\frac{dC}{dt}(t) = F_a C_a(t - T_a) + F_v C_v(t) - \frac{F_a + F_v}{V_e} C(t)$$

This model derives from the more general dual-inlet two-compartment uptake model by assuming the intracellular uptake rate is zero [13]. C , C_a , and C_v represent the concentrations in the tissue, aorta, and portal vein, respectively. The model is defined by three tissue parameters—arterial and venous plasma flows F_a and F_v , extracellular volume (ECV), and an arterial delay time T_a . The derived parameters are the total plasma flow ($F_p = F_a + F_v$), the extracellular mean transit time (MTT, $T_e = V_e / F_p$), and the arterial fraction (AF, $f_a = F_a / F_p$).

Fig. 1 Study flow. HCC = hepatocellular carcinoma, ICCA = intrahepatic cholangiocarcinoma, cHCC-CCA = combined hepatocellular carcinoma-cholangiocarcinoma, FNH = focal nodular hyperplasia



The model fit was performed using Levenberg-Marquardt least squares optimization with initial values $F_a = 10$ mL/min/100 mL, $F_v = 40$ mL/min/100 mL, and $V_e = 0.2$. Positivity constraints were enforced on all parameters and V_e was additionally constrained to be smaller than 1. The arterial delay time T_a was determined by repeating the fit for different values of T_a from 0 to 20 s in steps of 1 s, and we selected a value with the smallest chi-square fit error.

Histology

The specimens were fixed in a formalin-alcohol-acetic solution and were embedded in paraffin. Specimens were then cut into 4- μ m-thick sections and stained with hematoxylin-eosin. The liver fibrosis stage was assessed as follows: F0, no fibrosis; F1, portal fibrosis; F2, periportal fibrosis; F3, septal fibrosis; and F4, cirrhosis [18]. Tumors were diagnosed based on morphology in hematoxylin-eosin staining according to the 2010 World Health Organization Classification [19]. Immunohistochemistry analyses including heat shock protein 70, glypican 3, glutamine synthetase, cytokeratin-7, and cytokeratin-19 were performed when appropriate.

Outcomes

The primary endpoint is to make comparisons between portal blood flow at different hepatic fibrosis stages. A secondary endpoint is to draw comparisons between arterial blood flow at these fibrosis stages. In addition, we compared other DCE-MRI parameters across the fibrosis stages: comparing those with and without varices and comparing hepatocellular carcinomas (HCCs) with different LR categories. We also evaluated the image quality of the morphologic images to determine whether it is sufficient for clinical practice.

Statistical analysis

DCE-MRI parameters were compared among F0–F1, F2–F3, and F4 using a one-way ANOVA test followed by post hoc analyses using Bonferroni correction. A paired sample t test and a Student's t test were performed to compare the DCE-MRI parameters of HCC and liver parenchyma, and also compare HCCs with different LR features. Receiver operating characteristic curve analysis was used to assess the performance of DCE-MRI parameters to diagnose hepatic fibrosis \geq F2. The optimal cut-off values were calculated by maximizing the Youden index. The areas under the curve (AUCs) of parameters were compared using a χ^2 test. Inter-observer agreement was assessed using the intraclass correlation coefficient (ICC) and Bland-Altman plot. ICC was interpreted as follows: < 0.4 , poor; $0.4–0.59$, fair; $0.6–0.74$, good; and ≥ 0.75 , excellent [20]. All statistical analyses were performed using commercial software

(IBM SPSS, version 25, IBM; Medcalc version 19.6, Medcalc Software). A significance level of 0.05 was used.

Results

Sixty-four participants (male = 48; mean age, 56.4 ± 11 years) were analyzed after excluding five participants due to participant's withdrawal ($n = 1$), canceled operation ($n = 2$), or k-space data loss ($n = 2$) (Fig. 1). The fibrosis grades were F0 ($n = 21$), F1 ($n = 13$), F2 ($n = 9$), F3 ($n = 9$), and F4 ($n = 12$). 12.5% of participants (8/64) had varices and 35.9% (23/64) of participants had treatment-naïve HCCs. All hepatic observations were histologically confirmed. Detailed demographics are summarized in Table 1. The sizes of ROIs were 257 ± 269 voxels (range 42–1944) for AIF, 228 ± 147 (range 54–

Table 1 Demographics of study population

Variables	Values
Sex (M:F)	52:17
Age (years)	Male, 55.7 ± 10.7 (32, 82) Female, 57.9 ± 11.9 (23, 69)
Underlying disease	
Chronic hepatitis B	67.2% (43)
Chronic hepatitis C	12.5% (8)
Alcoholic cirrhosis	10.9% (7)
Cryptogenic cirrhosis	7.8% (5)
Biliary cirrhosis	1.6% (1)
Liver donor candidate	0% (0)
Diagnosis (resection:biopsy)	37:27
Fibrosis grade	
F0	32.8% (21)
F1	20.3% (13)
F2	14.1% (9)
F3	14.1% (9)
F4	18.8% (12)
Albumin	4.0 ± 0.5 (2.8, 5.1)
Total bilirubin	1.0 ± 0.7 (0.2, 3.8)
Prothrombin time (INR)	1.06 ± 0.11 (0.83, 1.56)
Hematocrit (%)	39.7 ± 0.7 (26.3, 51.1)
Hepatic observations	
None	29
Treated observations	8
Hepatocellular carcinoma (HCC)	23 (mean size, 33 ± 16 mm; range, 5, 71 mm)
Cholangiocarcinoma (CC)	1 (60 mm)
Combined HCC-CC	1 (47 mm)
FNH	1 (37 mm)
Hemangioma	1 (71 mm)

Values are mean \pm standard deviation (range) or percentage (number)
INR international normalized ratio, FNH focal nodular hyperplasia

Table 2 Qualitative analysis of image quality of dynamic phases

	Precontrast phase	Arterial phase	Portal venous phase	Delayed phase
Motion artifact	3.9 ± 0.2 (3.0, 4.0)	3.8 ± 0.2 (2.7, 4.0)	3.9 ± 0.2 (2.7, 4.0)	3.9 ± 0.2 (2.7, 4.0)
Streak artifact	2.9 ± 0.3 (2.0, 4.0)	3.4 ± 0.4 (2.3, 4.0)	3.5 ± 0.4 (2.0, 4.0)	3.4 ± 0.4 (2.0, 4.0)
Liver edge sharpness	3.6 ± 0.4 (2.7, 4.0)	3.5 ± 0.4 (2.7, 4.0)	3.7 ± 0.4 (2.7, 4.0)	3.7 ± 0.4 (2.3, 4.0)
Overall image quality	3.5 ± 0.4 (2.3, 4.0)	3.5 ± 0.4 (2.3, 4.0)	3.7 ± 0.4 (2.3, 4.0)	3.7 ± 0.4 (2.0, 4.0)

Values are mean ± standard deviation (range). A higher score indicates a better image quality

599) for VIF, 7227 ± 8751 (538–56175) for the liver, and 4381 ± 4960 (range 85–17,845) for the tumors.

Image quality evaluation and LR categorization

The average scores for overall image quality were 3.5 ± 0.4 in the precontrast and arterial phases and 3.7 ± 0.4 in the portal venous and delayed phases (Table 2, Fig. 2). No participant had an average score below two throughout the entire dynamic phase. Twenty-two treatment-naïve HCCs (≥ 10 mm) had LR-3 ($n = 5$), LR-5 ($n = 12$), and LR-M ($n = 5$) (Supplementary information).

Comparisons of DCE-MRI parameters among fibrosis stages

Compared to the participants with F0–F1, those with cirrhosis showed a significantly reduced portal blood flow (283 ± 178 vs. 98 ± 47 mL/100 mL/min, $p < 0.001$), a higher AF ($31.6 \pm$

25.2% vs. $56 \pm 16.2\%$, $p = 0.006$), a prolonged MTT (12 ± 10.4 s vs. 22.9 ± 9.2 s, $p = 0.002$), and an increased ECV (37 ± 11.3 vs. 48.1 ± 16.2 mL/100 mL, $p = 0.02$). Participants with F2–F3 also had a marginally lower AF ($35.4 \pm 19.7\%$, $p = 0.048$), shorter MTT (14.5 ± 5.4 s, $p = 0.046$), and lower ECV (35 ± 12 mL/100 mL, $p = 0.03$) than those in participants with F4 (Table 3).

The AUCs of portal blood flow, MTT, and AF for detecting clinically significant hepatic fibrosis (\geq F2) were 0.8, 0.77, and 0.7 respectively (Table 4). Portal blood flow showed a marginally higher AUC value than AF did ($p = 0.048$), but there were no significant differences between the AUCs for portal blood flow and MTT ($p = 0.4$) (Fig. 3).

Comparison of DCE-MRI parameters in the subgroups with and without varix

In participants with clinically significant hepatic fibrosis (\geq F2, $n = 30$), eight participants had varices. Compared to

Fig. 2 Free-breathing T1-weighted images in a 66-year-old man. Precontrast (a), arterial (b), portal-venous (c), and delayed phase (d) were obtained without breath-holding. Temporal resolution is 12 s. No significant motion artifact is observed in any of the phases. Approximately 4.8 cm HCC is shown in segment 7 (arrows)

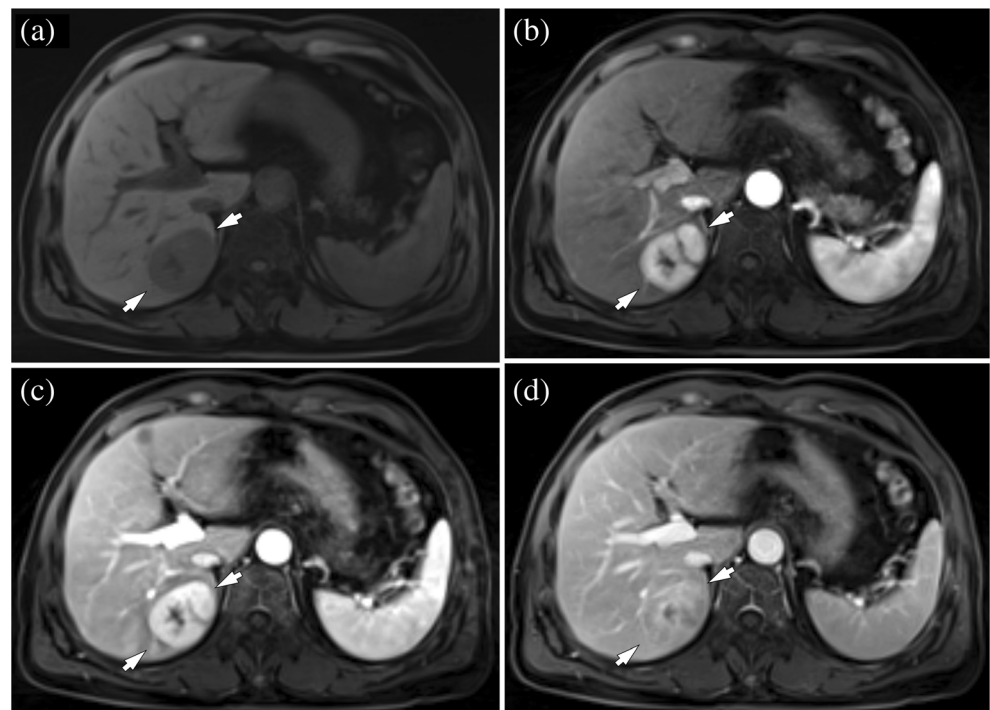


Table 3 Comparison of DCE-MRI variables in hepatic fibrosis

	F0-F1 (n = 34)	F2-F3 (n = 18)	F4 (n = 12)	<i>p</i> value		
				F0-F1 vs. F2-F3	F0-F1 vs. F4	F2-F3 vs. F4
Total blood flow (mL/100 mL/min)	405 ± 212 (112, 1047)	277 ± 137 (104, 604)	206 ± 93 (23, 391)	0.15		
Arterial blood flow (mL/100 mL/min)	122 ± 107 (23, 498)	102 ± 93 (11, 370)	126 ± 55 (59, 222)	0.73		
Portal blood flow (mL/100 mL/min)	283 ± 178 (0, 740)	175 ± 110 (53, 542)	98 ± 47 (14, 201)	0.04	0.001	0.48
Arterial fraction (%)	31.6 ± 25.2 (9.4, 100)	35.4 ± 19.7 (7.2, 76.4)	56 ± 16.2 (40.2, 94.0)	> 0.99	0.006	0.048
MTT (s)	12.0 ± 10.4 (3.6, 64.5)	14.5 ± 5.4 (7.8, 25.8)	22.9 ± 9.2 (11.6, 39.5)	> 0.99	0.002	0.046
ECV (mL/100 mL)	37 ± 11.3 (23.7, 85.8)	35.0 ± 12 (23.5, 67.1)	48.1 ± 16.2 (27.1, 72.6)	> 0.99	0.02	0.03

Values are mean ± standard deviation (range)

MTT mean transit time, *ECV* extracellular volume

participants without varices (n = 22), the variceal group showed a significantly higher AF (59.4 ± 25.4% vs. 37.9 ± 16%, *p* = 0.01) and increased ECV (55.3 ± 16.9 vs. 34.8 ± 9.9 mL/100 mL, *p* = 0.004). However, there was no significant difference of portal blood flow between the two groups (*p* = 0.24, Table E2).

Comparison of DCE-MRI parameters among HCCs with different imaging features

In twenty-three participants with treatment-naïve HCCs, two were excluded due to the small size (5 mm, n = 1) and substantial motion (segment 8 dome, n = 1). Compared with HCCs showing non-LR-M features (n = 16), HCCs with LR-M (n = 5) had a significantly prolonged MTT (22.4 ± 10.8 vs. 40.8 ± 10.8 s, respectively, *p* = 0.003) and lower arterial blood flow (277 ± 125 vs. 125 ± 25 mL/100 mL/min, respectively, *p* = 0.04) (Table 5, Figs. 4 and 5). HCCs demonstrated a significantly higher arterial blood flow, a decreased portal blood flow, a higher AF, a prolonged MTT, and an increased ECV when compared to the parenchyma (Table E3, *p* < 0.05 for all).

Inter-observer agreement

Inter-observer agreement was fair to good (0.57–0.62) for motion artifact, and good for streak artifact (0.61–0.69) and liver edge sharpness (0.67–0.74) in all phases. The overall image quality was good to excellent (0.63–0.75) in all phases (Supplementary information). The mean differences between the two observers were − 3.5 ± 39.4 mL/100 mL/min (limit of agreement (LOA): − 77.3, 70.3) for portal blood flow, 0.2 ± 6.9% (LOA: − 13.6, 13.9) for AF, − 1.7 ± 14.1 s (LOA: − 27.7, 24.4) for MTT, and − 0.1 ± 4.6 mL/100 mL (LOA: − 8.9, 8.7) for ECV.

Discussion

Our study showed that portal blood flow was significantly reduced in clinically significant hepatic fibrosis (≥ F2) compared with that in participants with no or early hepatic fibrosis. Conversely, there were no significant differences in arterial blood flow among the fibrosis stages. The reduction in portal flow associated with advanced hepatic fibrosis is often

Table 4 Diagnostic performance for diagnosing clinically significant hepatic fibrosis (≥ F2)

	AUC	Cut-off value	Sensitivity (%)	Specificity (%)	<i>p</i> value
Portal blood flow (mL/100 mL/min)	0.80 (0.68, 0.89)	≤ 147	73.3 (54.1, 87.7)	85.3 (68.9, 95)	< 0.001
Arterial fraction (%)	0.70 (0.57, 0.81)	> 38.8	60 (40.6, 77.3)	79.4 (62.1, 91.3)	0.003
MTT (s)	0.77 (0.64, 0.86)	> 9.3	96.7 (82.8, 99.9)	52.9 (35.1, 70.2)	< 0.001
ECV (mL/100 mL)	0.52 (0.39, 0.64)	> 30.2	60 (40.6, 77.3)	20.6 (8.7, 37.9)	0.84

Values in parenthesis are 95% confidence interval

AUC area under the curve, *MTT* mean transit time, *ECV* extracellular volume

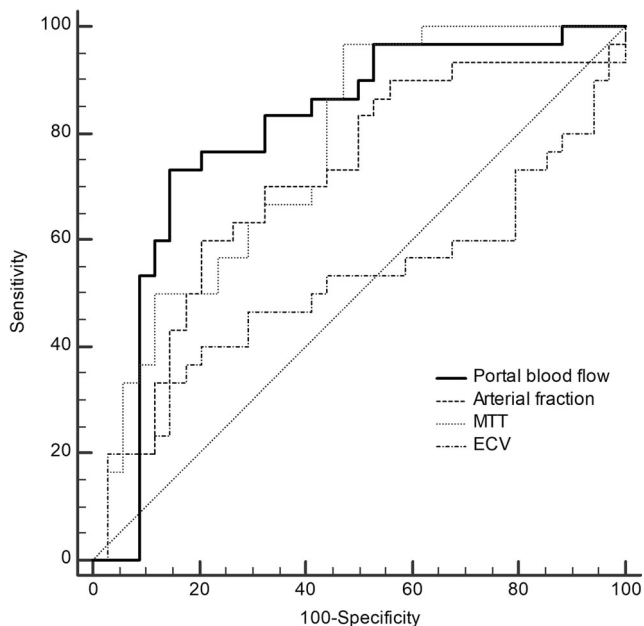


Fig. 3 Diagnostic performance of DCE-MRI parameters for diagnosing clinically significant hepatic fibrosis (\geq F2). Areas under the curve (AUCs) of portal blood flow, arterial fraction (AF), mean transit time (MTT), and extracellular volume (ECV) are 0.8, 0.7, 0.77, and 0.52 respectively. There are no significant differences between the AUCs of portal blood flow, AF, and MTT

explained by the increased intrahepatic resistance [21, 22]: the increased hepatic vascular tone and the alteration of tissue architecture by collagen deposition in the space of Disse may increase intrahepatic resistance [23, 24]. The absence of any significant differences in arterial blood flow may be explained via the so-called buffer phenomenon, in which a reduced portal flow is compensated by an increased arterial flow—which in turn increases AF [25]. We also observed increased MTTs and ECVs in participants with cirrhosis. MTT is the average time for blood to transit from the arterial to the venous end of the vasculature, and ECV refers to interstitial space volume. Given that collagen deposit increases and sinusoid capillarization occurs in cirrhosis [26], a prolonged

MTT and increased ECV in cirrhosis are perhaps unsurprising outcomes. Based on our observations, we cautiously suggest that the hemodynamic changes in hepatic fibrosis can be captured via DCE-MRI.

The prognosis of patients with advanced chronic liver disease depends on the development of portal hypertension [27], and the presence of varices is an indirect metric of portal hypertension [28]. We found that AFs and ECVs were significantly higher in the group with varices compared to the non-variceal group. However, contrary to expectations, there were no significant differences in portal flow between the two groups. Although the reasons for this are not clear, we can speculate that it may be explained by portal hyperemia. Despite the flow divergence caused by collaterals, arterial vasodilatation of the splanchnic and systemic circulation increases splanchnic flow to the portal system [29]. As a result, portal flow may increase in the variceal group and ultimately result in there being no significant difference between the two groups. The potential role DCE-MRI for portal hypertension evaluation should be further investigated in the future with an appropriate reference of portal hypertension.

Our study shows the feasibility of simultaneous evaluation of both morphologic and hepatic perfusion in a single examination. In our study, no participants underwent re-examinations, and this motion-resistant sequence also allowed DCE-MRI analyses for hepatic tumors: the HCCs had significantly higher arterial blood flow, markedly lower portal blood flow, longer MTT, and greater ECV than those of the liver parenchyma. This is consistent with the known hemodynamics of HCCs, and the prolonged MTT can also be explicated by the tortuous neovascularity of the tumor [30, 31]. Of interest, HCCs with different imaging features showed different perfusion parameters. HCCs with LR-M had significantly lengthened MTTs and a lower total and arterial blood flow than those in non-LR-M HCCs. Given that HCCs with LR-M do not show typical arterial phase hyperenhancement, it is coherent to conclude that those subjective imaging features can be quantified via DCE-MRI. Because HCCs with LR-M are known to be associated

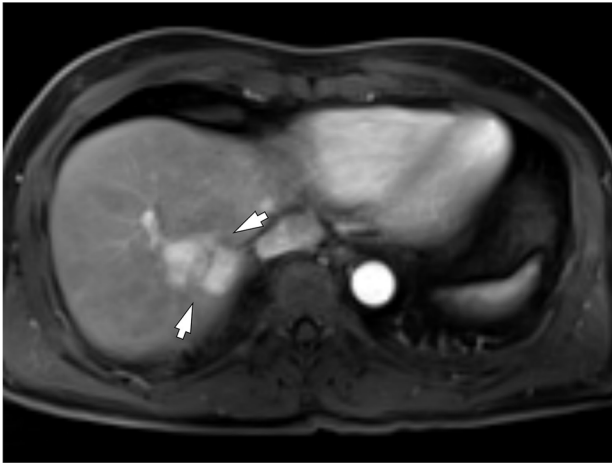
Table 5 Comparison of DCE-MRI parameters between hepatocellular carcinomas with different LI-RADS features

	HCCs with non-LR-M (n = 16)*	HCCs with LR-M (n = 5)	p value
Total blood flow (mL/100 mL/min)	294 ± 208 (85, 860)	128 ± 26 (98, 162)	0.04
Arterial blood flow (mL/100 mL/min)	277 ± 125 (85, 729)	125 ± 25 (98, 162)	0.04
Portal blood flow (mL/100 mL/min)	17 ± 37 (0, 130)	3 ± 6 (0, 13)	0.36
Arterial fraction (%)	95.9 ± 7.6 (76.2, 100)	98.2 ± 3.9 (91.2, 100)	0.51
MTT (s)	22.4 ± 10.8 (7.4, 38.5)	40.8 ± 10.8 (31.7, 59)	0.003
ECV (mL/100 mL)	56.8 ± 24.5 (22.3, 100)	50.8 ± 13 (36, 69.6)	0.61

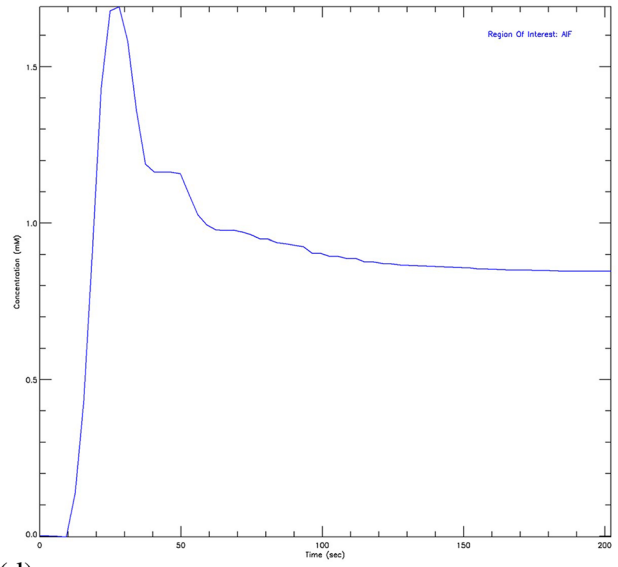
HCC hepatocellular carcinoma, LI-RADS Liver Imaging Reporting and Data System, MTT mean transit time, ECV extracellular volume

*Four participants with LR-3 and twelve participants with LR-5

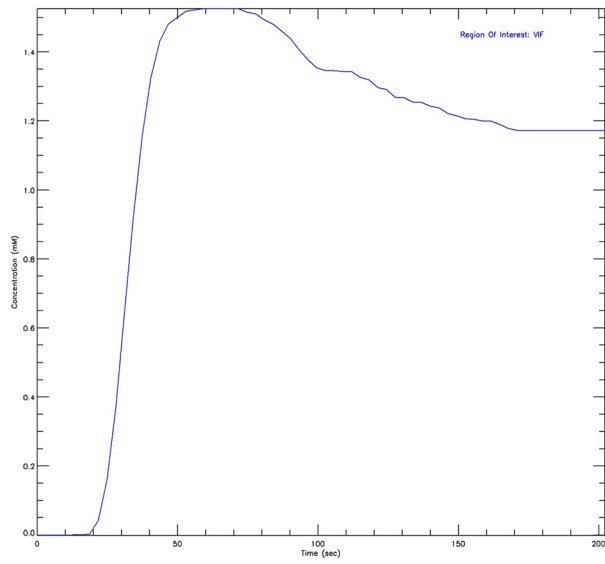
(a)



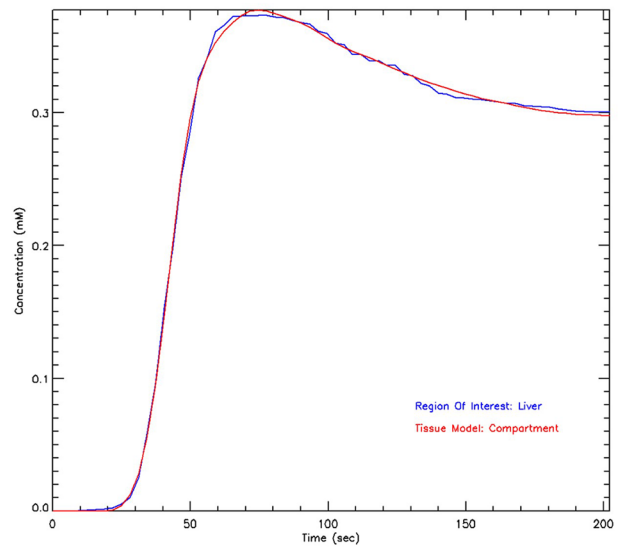
(b)



(c)



(d)



(e)

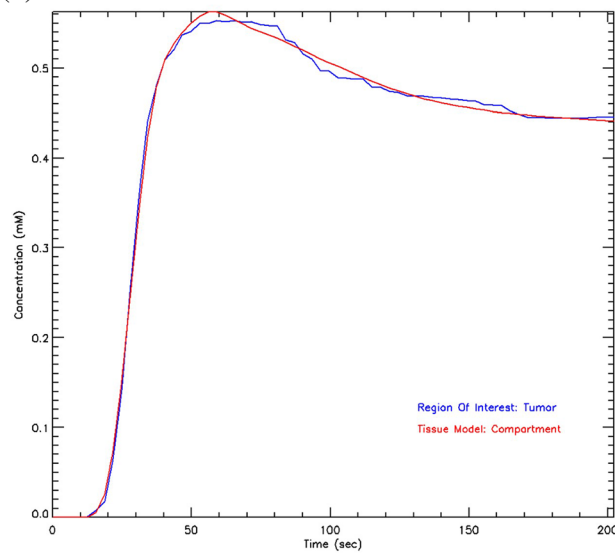


Fig. 4 A 53-year-old man with F4. Approximately 4 cm HCC with LR-5 shows arterial phase hyperenhancement (a, arrows) and portal washout (not shown). Arterial input function (b), venous input function (c), and the fitting curves of liver parenchyma (d) and HCC (e) are presented. Portal blood flow is 125 mL/100 mL/min in liver parenchyma and 0 mL/100 mL/min in the tumor. AF is 47.8% in the liver and 100% in HCC

with poor prognosis [32], there might be a role of DCE-MRI for tumor biology characterization. We believe that GRASP can provide the additional hemodynamic information, in combination with an appropriate analysis model.

Despite our study results being consistent with previous studies reporting both a reduced portal flow and an increased AF and MTT [4, 33, 34], the absolute values of liver blood

flow in this study are higher than the reported values: a typical value for total blood flow in healthy liver is in the range of 130 mL/min/100 mL [35, 36], but in this study, we measured an average of 405 mL/min/100 mL in the F0–F1 group. This may reflect a systematic overestimation in the data. The reason is not clear, but using a constant T1 value may be partly responsible for this since the T1 value changes as fibrosis progresses. In addition, inspection of a typical AIF demonstrates that the peak concentration is saturated, which has been also shown in other studies using radial acquisition [31, 37, 38]. A possible contributor to this effect is the relatively low flip angle (12°), which is necessary to minimize power deposition but is also known to reduce the dynamic range of the signal in radial acquisition [39]. One would not expect the effect to be so

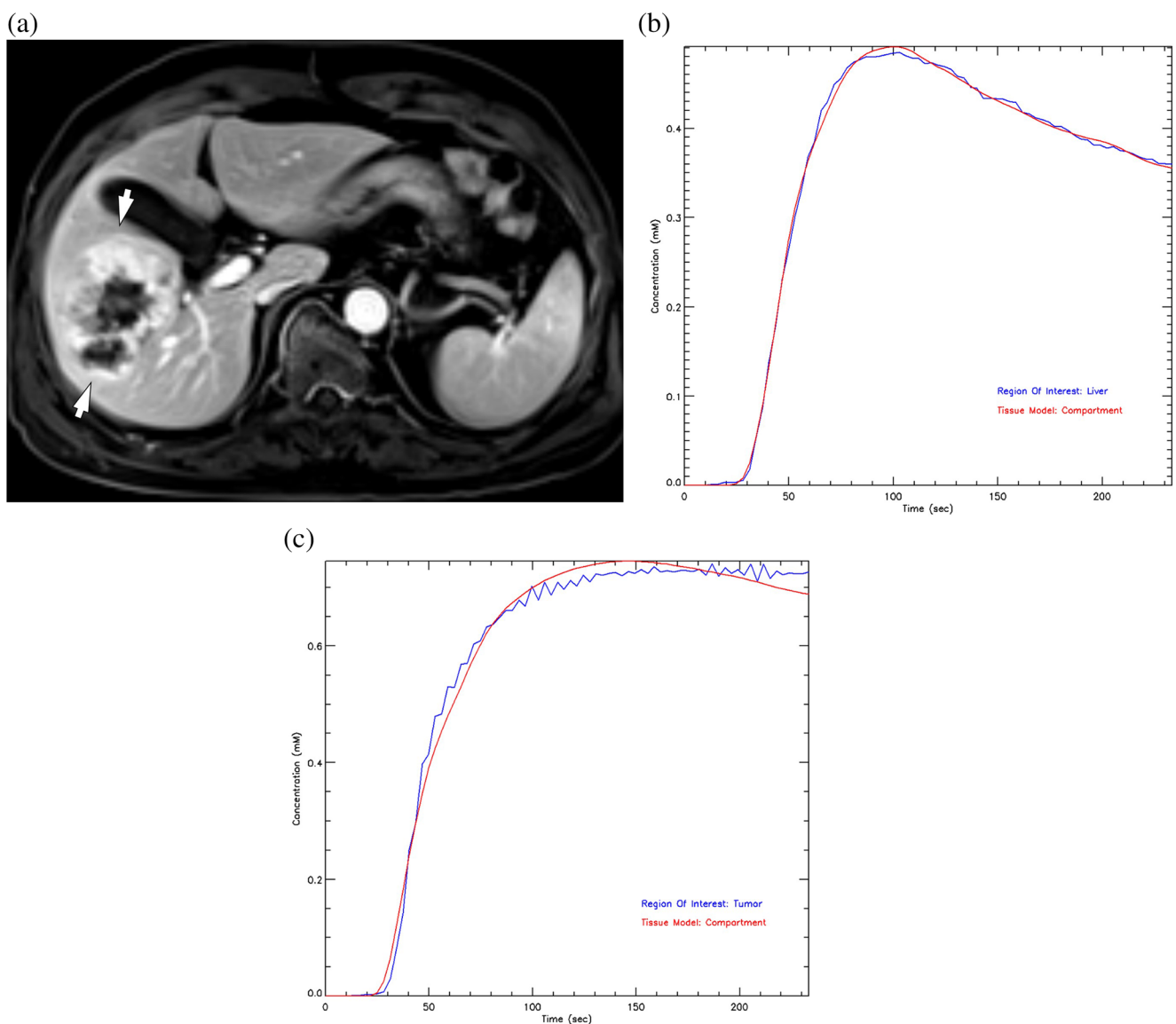


Fig. 5 A 79-year-old man with F2. Approximately 5.7 cm HCC with LR-M feature (a, arrows) is in segment 5. Fitting curve of liver parenchyma (b) and HCC (c) are presented. Portal blood flow is 147 mL/100 mL/min

in liver parenchyma and 0 mL/100 mL/min in the tumor. AF is 27% in the liver and 100% in HCC

severe at 12°, and therefore, it seems likely that other issues play a role such as, potentially, temporal smoothness constraints, temporal resolution (the number of spokes), and principal component of GRASP reconstruction [40, 41]. The effect is likely to be largely systematic in nature and therefore may not confound the cross-sectional comparisons, but it will certainly impact on the reproducibility of the results and the ability to make comparisons against benchmarks and reference methods. Further investigation including population-based AIF and B1-corrected T1 mapping is needed to address this potential obstacle in DCE-MRI using radial acquisition.

There are several study limitations. First, the sample size was relatively small. Second, participants with different underlying diseases were enrolled. Third, we used a constant T1 value to avoid errors related to B1-effects. However, precise T1 measurement should be implemented in the following studies. Third, we applied dual-input model for HCCs. It is based on the fact that the degree of portal flow reduction varies in HCCs, and we decided to include portal contribution as in earlier studies [42, 43]. However, the gain of using a dual-input model over a single-input model is not yet validated in HCCs. Further, there are concerns about the fact that the dual-input model may increase the instability of the model fit and decrease the reliability of other perfusion parameters. Lastly, the presence of varices is only a surrogate marker of portal hypertension. Further studies including solid reference standards such as hepatic venous pressure gradients are warranted.

In conclusion, DCE-MRI can be simultaneously obtained with morphologic imaging from a single acquisition dataset, and portal blood flow significantly differed between fibrosis stages.

Supplementary Information The online version contains supplementary material available at <https://doi.org/10.1007/s00330-021-08087-2>.

Acknowledgements We thank Benjamin Latimer, BA, for his editorial assistance.

Funding This study was supported by Basic Science Research Program through the National Research Foundation of Korea funded by the Ministry of Education (2013R1A1A2A10066037).

Declarations

Guarantor The scientific guarantor of this publication is Professor Jeong Min Lee.

Conflict of interest Two authors (R. Grimm and Y. Son) are employees of Siemens Healthineers. Otherwise, the authors of this manuscript declare no relationships with any companies whose products or services may be related to the subject matter of the article.

Statistics and biometry No complex statistical methods were used for this paper.

Informed consent Written informed consent was obtained from all participants.

Ethical approval Approval from the Institutional Review Board of Seoul National University Hospital was obtained.

Methodology

- prospective
- cross-sectional study
- performed at one institution


References

1. Shin GW, Zhang Y, Kim MJ et al (2018) Role of dynamic contrast-enhanced MRI in evaluating the association between contralateral parenchymal enhancement and survival outcome in ER-positive, HER2-negative, node-negative invasive breast cancer. *J Magn Reson Imaging* 48:1678–1689
2. Li KL, Lewis D, Jackson A, Zhao S, Zhu X (2018) Low-dose T1W DCE-MRI for early time points perfusion measurement in patients with intracranial tumors: A pilot study applying the microsphere model to measure absolute cerebral blood flow. *J Magn Reson Imaging* 48:543–557
3. Cristel G, Esposito A, Damascelli A et al (2019) Can DCE-MRI reduce the number of PI-RADS v.2 false positive findings? Role of quantitative pharmacokinetic parameters in prostate lesions characterization. *Eur J Radiol* 118:51–57
4. Hagiwara M, Rusinek H, Lee VS et al (2008) Advanced liver fibrosis: diagnosis with 3D whole-liver perfusion mr imaging—initial experience1. *Radiology* 246:926–934
5. San Koh T, Thng CH, Lee PS et al (2008) Hepatic metastases: in vivo assessment of perfusion parameters at dynamic contrast-enhanced MR imaging with dual-input two-compartment tracer kinetics model1. *Radiology* 249:307–320
6. Pandharipande PV, Krinsky GA, Rusinek H, Lee VS (2005) Perfusion imaging of the liver: current challenges and future goals. *Radiology* 234:661–673
7. Winkel DJ, Heye TJ, Benz MR et al (2019) Compressed sensing radial sampling MRI of prostate perfusion: utility for detection of prostate cancer. *Radiology* 290:702–708
8. Gill AB, Black RT, Bowden DJ, Priest AN, Graves MJ, Lomas DJ (2014) An investigation into the effects of temporal resolution on hepatic dynamic contrast-enhanced MRI in volunteers and in patients with hepatocellular carcinoma. *Phys Med Biol* 59:3187–3200
9. Chandarana H, Feng L, Ream J et al (2015) Respiratory motion-resolved compressed sensing reconstruction of free-breathing radial acquisition for dynamic liver magnetic resonance imaging. *Invest Radiol* 50:749–756
10. Chandarana H, Feng L, Block TK et al (2013) Free-breathing contrast-enhanced multiphase MRI of the liver using a combination of compressed sensing, parallel imaging, and golden-angle radial sampling. *Invest Radiol* 48:10–16
11. Yoon JH, Lee JM, Yu MH et al (2018) Evaluation of transient motion during gadoteric acid-enhanced multiphasic liver magnetic resonance imaging using free-breathing golden-angle radial sparse parallel magnetic resonance imaging. *Invest Radiol* 53:52–61
12. Chernyak V, Fowler KJ, Kamaya A et al (2018) Liver Imaging Reporting and Data System (LI-RADS) Version 2018: imaging of hepatocellular carcinoma in at-risk patients. *Radiology* 289:816–830
13. Sourbron S, Sommer WH, Reiser MF, Zech CJ (2012) Combined quantification of liver perfusion and function with dynamic gadoteric acid-enhanced MR imaging. *Radiology* 263:874–883

14. Juluru K, Talal AH, Yantiss RK et al (2017) Diagnostic accuracy of intracellular uptake rates calculated using dynamic Gd-EOB-DTPA-enhanced MRI for hepatic fibrosis stage. *J Magn Reson Imaging* 45:1177–1185
15. Armbruster M, Sourbron S, Haug A et al (2014) Evaluation of neuroendocrine liver metastases: a comparison of dynamic contrast-enhanced magnetic resonance imaging and positron emission tomography/computed tomography. *Invest Radiol* 49:7–14
16. Stanisz GJ, Odobina EE, Pun J et al (2005) T1, T2 relaxation and magnetization transfer in tissue at 3T. *Magn Reson Med* 54:507–512
17. Lu H, Clingman C, Golay X, van Zijl PC (2004) Determining the longitudinal relaxation time (T1) of blood at 3.0 Tesla. *Magn Reson Med* 52:679–682
18. Park YN, Chon CY, Park JB et al (1999) Histological grading and staging of chronic hepatitis standardized guideline proposed by the Korean Study Group for the Pathology of Digestive Diseases. *Korean J Pathol* 33:337–346
19. Bosman FTFC, Hruban RH, Theise ND (2010) WHO classification of tumours. *Digestive System Tumours*, 5th edn. World Health Organization, Geneva, Switzerland
20. Ueno Y, Maeda T, Tanaka U et al (2016) Evaluation of interobserver variability and diagnostic performance of developed MRI-based radiological scoring system for invasive placenta previa. *J Magn Reson Imaging* 44:573–583
21. Groszmann R, Kotlanski B, Cohn JN, Khatri IM (1972) Quantitation of portosystemic shunting from the splenic and mesenteric beds in alcoholic liver disease. *Am J Med* 53:715–722
22. Kotlanski B, Groszmann R, Cohn JN (1972) Circulation times in the splanchnic and hepatic beds in alcoholic liver disease. *Gastroenterology* 63:102–111
23. Iredale JP (2007) Models of liver fibrosis: exploring the dynamic nature of inflammation and repair in a solid organ. *J Clin Invest* 117:539–548
24. Berzigotti A, Bosch J (2014) Pharmacologic management of portal hypertension. *Clin Liver Dis* 18:303–317
25. Greenway CV, Lawson AE, Stark RD (1967) The effect of haemorrhage on hepatic artery and portal vein flows in the anesthetized cat. *J Physiol* 193:375–379
26. Poisson J, Lemoine S, Boulanger C et al (2017) Liver sinusoidal endothelial cells: physiology and role in liver diseases. *J Hepatol* 66:212–227
27. Bosch J, Garcia-Pagan JC (2000) Complications of cirrhosis I. Portal hypertension. *J Hepatol* 32:141–156
28. Lee DH, Ahn JH, Chung JW et al (2019) Varices on computed tomography are surrogate of clinically significant portal hypertension and can predict survival in compensated cirrhosis patients. *J Gastroenterol Hepatol* 34:450–457
29. Iwakiri Y (2014) Pathophysiology of portal hypertension. *Clin Liver Dis* 18:281–291
30. Okada M, Kim T, Murakami T (2011) Hepatocellular nodules in liver cirrhosis: state of the art CT evaluation (perfusion CT/volume helical shuttle scan/dual-energy CT, etc.). *Abdom Imaging* 36:273–281
31. Weiss J, Ruff C, Grosse U et al (2019) Assessment of hepatic perfusion using GRASP MRI: bringing liver MRI on a new level. *Invest Radiol* 54:737–743
32. Choi SH, Lee SS, Park SH et al (2019) LI-RADS classification and prognosis of primary liver cancers at gadoteric acid-enhanced MRI. *Radiology* 290:388–397
33. Leporq B, Dumortier J, Pilleul F, Beuf O (2012) 3D-liver perfusion MRI with the MS-325 blood pool agent: a noninvasive protocol to assess liver fibrosis. *J Magn Reson Imaging* 35:1380–1387
34. Ou HY, Bonekamp S, Bonekamp D et al (2013) MRI arterial enhancement fraction in hepatic fibrosis and cirrhosis. *AJR Am J Roentgenol* 201:W596–W602
35. Bradley SE (1949) Variations in hepatic blood flow in man during health and disease. *N Engl J Med* 240:456–461
36. Feng AC, Fan HL, Chen TW, Hsieh CB (2014) Hepatic hemodynamic changes during liver transplantation: a review. *World J Gastroenterol* 20:11131–11141
37. Parikh N, Ream JM, Zhang HC, Block KT, Chandarana H, Rosenkrantz AB (2016) Performance of simultaneous high temporal resolution quantitative perfusion imaging of bladder tumors and conventional multi-phase urography using a novel free-breathing continuously acquired radial compressed-sensing MRI sequence. *Magn Reson Imaging* 34:694–698
38. Eikefjord E, Andersen E, Hodneland E et al (2015) Use of 3D DCE-MRI for the estimation of renal perfusion and glomerular filtration rate: an intrasubject comparison of FLASH and KWIC with a comprehensive framework for evaluation. *AJR Am J Roentgenol* 204:W273–W281
39. Wake N, Chandarana H, Rusinek H et al (2018) Accuracy and precision of quantitative DCE-MRI parameters: how should one estimate contrast concentration? *Magn Reson Imaging* 52:16–23
40. Mansour R, Thibodeau Antonacci A, Bilodeau L et al (2020) Impact of temporal resolution and motion correction for dynamic contrast-enhanced MRI of the liver using an accelerated golden-angle radial sequence. *Phys Med Biol* 65:085004
41. Feng L, Wen Q, Huang C, Tong A, Liu F, Chandarana H (2020) GRASP-Pro: improving GRASP DCE-MRI through self-calibrating subspace-modeling and contrast phase automation. *Magn Reson Med* 83:94–108
42. Hectors SJ, Lewis S, Kennedy P et al (2020) Assessment of hepatocellular carcinoma response to (90)Y radioembolization using dynamic contrast material-enhanced MRI and intravoxel incoherent motion diffusion-weighted imaging. *Radiol Imaging Cancer* 2: e190094
43. Ghodasara S, Chen Y, Pahwa S et al (2020) Quantifying perfusion properties with DCE-MRI using a dictionary matching approach. *Sci Rep* 10:10210

Publisher's note Springer Nature remains neutral with regard to jurisdictional claims in published maps and institutional affiliations.

Affiliations

Jeong Hee Yoon^{1,2} · Jeong Min Lee^{1,2,3}  · Mi Hye Yu⁴ · Bo Yun Hur⁵ · Robert Grimm⁶ · Steven Sourbron⁷ · Hersh Chandarana^{8,9} · Yohan Son¹⁰ · Susmita Basak¹¹ · Kyoung-Bun Lee¹² · Nam-Joon Yi¹³ · Kwang-Woong Lee¹³ · Kyung-Suk Suh¹³

¹ Radiology, Seoul National University Hospital, 101 Daehak-ro, Jongno-gu, Seoul 03080, Republic of Korea

² Seoul National University College of Medicine, 101 Daehak-ro, Jongno-gu, Seoul 03080, Republic of Korea

- ³ Institute of Radiation Medicine, Seoul National University Medical Research Center, 103 Daehak-ro, Jongno-gu, Seoul 03087, Republic of Korea
- ⁴ Radiology, Konkuk University School of Medicine, Seoul 05080, Republic of Korea
- ⁵ Radiology, Seoul National University Hospital Healthcare System Gangnam Center, Seoul 06236, Republic of Korea
- ⁶ Siemens Healthineers, 91052 Erlangen, Germany
- ⁷ Infection, Immunity and Cardiovascular Disease, University of Sheffield, Sheffield, UK
- ⁸ Center for Advanced Imaging Innovation and Research (CAI2R), New York, NY, USA
- ⁹ Department of Radiology, New York University Grossman School of Medicine, New York, NY 10016, USA
- ¹⁰ Siemens Healthcare Korea, Seoul 03737, Republic of Korea
- ¹¹ Biomedical Imaging Sciences Department, Leeds Institute of Cardiovascular and Metabolic Medicine, University of Leeds, Leeds, UK
- ¹² Pathology, Seoul National University College of Medicine, 103 Daehak-ro, Jongno-gu, Seoul 03087, Republic of Korea
- ¹³ Surgery, Seoul National University College of Medicine, 103 Daehak-ro, Jongno-gu, Seoul 03087, Republic of Korea